Contrast and resolution in imaging with a microfocus x-ray source

A. Pogany,[a] D. Gao, and S. W. Wilkins
CSIRO, Division of Materials Science & Technology, PB33 Clayton South MDC, Vic 3169, Australia

(Received 3 February 1997; accepted for publication 21 April 1997)

A simple general treatment of x-ray image formation by Fresnel diffraction is presented; the image can alternatively be considered as an in-line hologram. Particular consideration is given to phase-contrast microscopy and imaging using hard x rays. The theory makes use of the optical transfer function in a similar way to that used in the theory of electron microscope imaging. Resolution and contrast are the criteria used to specify the visibility of an image. Resolution in turn depends primarily on the spatial coherence of the illumination, with chromatic coherence of lesser importance. Thus broadband microfocus sources can give useful phase-contrast images. Both plane- and spherical-wave conditions are explicitly considered as limiting cases appropriate to macroscopic imaging and microscopy, respectively, while intermediate cases may also be of practical interest. Some results are presented for x-ray images showing phase contrast. © *1997 American Institute of Physics.* [S0034-6748(97)04907-1]

I. INTRODUCTION

For 100 years x-ray imaging has depended almost wholly on the phenomenon of absorption by an object to produce contrast. For light optics (particularly microscopy) on the other hand, phase-contrast has been appreciated and used for at least 60 years.[1] High-resolution transmission electron microscopy (TEM) has also relied on phase contrast in imaging for at least 30 years, although for technical reasons a different type of phase contrast is used.[2,3] Over the same time various methods for x-ray phase-contrast imaging have been proposed and demonstrated, particularly over the last few years with the increasing use of synchrotron sources. They have involved either Bonse–Hart monolithic x-ray interferometers,[4–6] double-crystal diffraction arrangements,[7–10] Fresnel or Bragg–Fresnel lenses,[11–13] or Fresnel diffraction from a monochromatic source.[14,15] These methods all seem to require rather elaborate optics. On the other hand, a simple approach to phase-contrast imaging with hard x-rays is possible, which also uses Fresnel diffraction to provide contrast, but requires only a moderately coherent source such as can be produced by a conventional x-ray tube.[16]

Soon after the introduction of holography[17] by Gabor in 1948, the possibility of x-ray holography was explored,[18] and interest has continued, mainly in the context of soft x-ray microscopy.[19–35] As is well known, the hologram contains phase information from the object wave field, so that it may be considered in a sense as a phase-contrast image, i.e., the phase has been ''made visible,'' although a reconstruction step is required to reproduce the phase distribution at the object. From a different viewpoint, the reconstruction may be considered as a form of phase retrieval.[36–39]

Another form of x-ray microscopy, namely point-projection microscopy (or microradiography) was developed somewhat earlier.[40,41] The experimental arrangement is the same as for point-source in-line holography, but applied to absorbing objects, which produce a shadow image. Fresnel diffraction in this case is considered as undesirable image blurring.

In the present article a simple theoretical framework is presented to treat Fresnel diffraction imaging by x-rays (including in-line holography) as embodied in the various cases mentioned above, namely:

(i) macro- and microscopic imaging,
(ii) phase and amplitude objects, and
(iii) plane- and spherical-wave geometry.

The emphasis however is on phase contrast. The theory treats Fresnel diffraction effectively in terms of its optical transfer function (OTF), and is based largely on that commonly used for high-resolution TEM imaging.[2,3] Resolution and contrast are considered as the two factors controlling image quality (or ''visibility''). Resolution in turn is largely determined by coherence considerations (Sec. III) rather than by the diffraction-limited conditions of conventional optics.

In Sec. IV our findings are discussed, and an illustration of phase-contrast x-ray imaging is presented. Section V contains a summary.

II. THEORY

Let a thin object lying in the plane $z=0$ be illuminated with a monochromatic plane wave $\exp\{-ikz\}$. The wave function just beyond the object is given by the transmission function $q(x)$ [we assume a one dimensional object for convenience but there is no difficulty in extending the following treatment to a two dimensional object, $q(x,y)$, etc] On further planes $z>0$, the wave function $f(x;z)$ is given by Fresnel diffraction theory. In particular, if the relevant features of the object are large compared to the wavelength $\lambda(=2\pi/k)$ one can apply the usual small angle (i.e., paraxial) approximations to obtain the Fresnel–Kirchhoff integral[1]

[a]Electronic mail: pogany@mst.csiro.au

 0034-6748/97/68(7)/2774/9/$10.00

$$f(x;z)=\left(\frac{i}{\lambda z}\right)^{1/2}\exp(-ikz)\int q(X)\times\exp\left(\frac{-ik(x-X)^2}{2z}\right)dX. \tag{1}$$

The integral is of convolution type which suggests Fourier transformation (FT) with respect to x, giving

$$F(u;z)=\exp(-ikz)Q(u)\exp(i\pi\lambda z u^2). \tag{2}$$

Here F and Q are the one dimensional FTs of f and q, respectively. The z dependence is explicitly retained. The variable u represents spatial frequency at the object or image plane. Here and subsequently ''image'' is used in the generalized sense of a defocused image. The function $\exp\{i\pi\lambda z u^2\}$ is effectively the optical transfer function for Fresnel diffraction and may also be thought of as a *linear filter* acting on the transmitted frequencies.[1] In the present case it has unit modulus, meaning that there is in a formal sense no loss of information involved in Fresnel diffraction, although this holds only within the small-angle approximation and does not extend to indefinitely large spatial frequencies. However, not all the information is realized in the image intensities.

The transmission function, $q(x)$, may be written

$$q(x)=\exp[i\phi(x)-\mu(x)] \tag{3}$$

displaying the absorption and phase-shift components of the object (μ is the z projection of half the usual linear attenuation coefficient for the intensity). If these are small,

$$q(x)\approx 1+i\phi(x)-\mu(x) \tag{4}$$

and

$$F(u)\approx[\delta(u)+i\Phi(u)-m(u)]\exp[i\chi(u)] = \delta(u)-\Phi\ \sin\chi-m\ \cos\chi+i(\Phi\ \cos\chi-m\ \sin\chi), \tag{5}$$

where $\chi(u)=\pi\lambda z u^2$, and m and Φ are the FTs of μ and ϕ, respectively.

Following the treatment given in Ref. 2, we obtain from Eq. (5)

$$f(x)\approx 1-\mu*\mathscr{F}\cos\chi-\phi*\mathscr{F}\sin\chi +i(\phi*\mathscr{F}\cos\chi-\mu*\mathscr{F}\sin\chi), \tag{6}$$

where $\mathscr{F}$ indicates a FT and * a convolution. To first order in ϕ, μ, the intensity can be written as

$$I(x)=|f(x)|^2\approx 1-2\mu*\mathscr{F}\cos\chi-2\phi*\mathscr{F}\sin\chi \tag{7}$$

and so, to this order,

$$F(u)\approx\delta(u)-m(u)\cos\chi-\Phi(u)\sin\chi. \tag{8}$$

Thus the real and imaginary parts of the OTF have a simple interpretation in terms of image contrast of the amplitude and phase components of the object transmission function, and are used primarily in treatments of electron microscope imaging,[2,3] where phase contrast is commonly produced by defocusing. Referring to intensity rather than amplitude, one should more correctly use the term ''contrast transfer function'' (CTF), but we shall continue to use OTF to refer to either case. In conventional light optics the modulus and phase of the OTF are more usually considered.

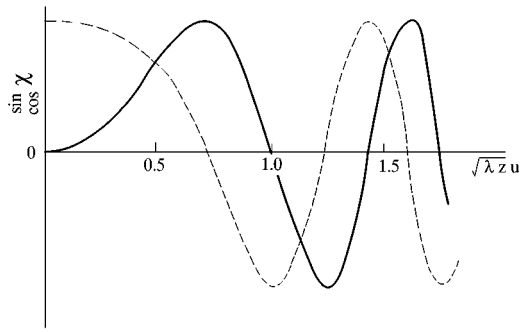

FIG. 1. Real (dashed) and imaginary (solid line) parts of the Fresnel diffraction optical transfer function vs. reduced spatial frequency $u'=(\lambda z)^{1/2}u$.

$\sin\chi$ and $\cos\chi$ can be conveniently plotted against the reduced variable $u'=(\lambda z)^{1/2}u$ as shown in Fig. 1.

Let us now consider a weak phase object so that

$$F(u)\approx\delta(u)-\Phi(u)\sin\chi. \tag{9}$$

For sufficiently small u', $\sin\chi\approx\chi$ and (9) becomes

$$F(u)=\delta(u)-\pi\lambda z u^2\Phi(u) \tag{10}$$

giving for the intensity[2]

$$I(x)\approx 1+\frac{\lambda z}{2\pi}\phi''(x). \tag{11}$$

Thus in this regime contrast is proportional to the second derivative (Laplacian in the two dimensional case) of the phase function. For electrons, ϕ is proportional to the z-projected electrostatic potential of the object, and hence, from Poisson's equation contrast is proportional to the *projected charge density*[42]

$$\rho(x)\approx\int\rho(x,z)dz. \tag{12}$$

For x rays[8]

$$\phi(x)=r_e\lambda\rho_e(x), \tag{13}$$

where r_e is the classical electron radius and ρ_e the *projected electron density* (at least away from absorption edges), so that

$$I(x)\approx 1-\frac{\lambda^2}{2\pi}r_e z\rho_e''(x). \tag{14}$$

Here the contrast is proportional to the Laplacian of the projected electron density, so variations in projected electron density will show up preferentially, e.g., features will show enhanced edge contrast, while low spatial frequencies (phase changes with little spatial variation) will have low contrast; hence the term *differential phase contrast* for this type of image.

Two other features of Eq. (14) may be noted:

(i) the *contrast in the image increases directly with* z,
(ii) the wavelength appears only as a separable factor

λ^2. The geometric features of the contrast are *wavelength independent*, which means that polychromatic radiation may equally well be used:[16] the factor λ^2 is then replaced by a spectrally weighted sum.

For large u' it may be noted that sin χ reaches its first maximum at $u'=\sqrt{1/2}$ [i.e., $(2\lambda z)^{1/2}u=1$], and for u values in this region, sin $\chi\approx 1$,

$$F(u)\approx\delta(u)-\Phi(u), \tag{15}$$

$$I(x)\approx 1-2\phi(x), \tag{16}$$

and in particular for x rays

$$I(x)=1-2r_e\lambda\rho_e(x), \tag{17}$$

i.e., the phase (or projected electron density) itself, rather than its Laplacian, appears in the contrast term in this regime. As before, λ appears simply as a multiplier so again the image structural features are wavelength independent to a reasonable approximation. For example, if $\lambda=0.1$ nm, $z=0.5$ m, the maximum phase contrast will occur for $u=10^5$ m^{-1}, i.e., for spacings, d, around 10 μm. Spatial frequencies much less than this will give only weak contrast. For higher spatial frequencies there are further ''pass bands'', e.g., the next around $u'=(3/2)^{1/2}$ showing reverse contrast ($u\approx 1.7\times 10^5$ m^{-1}, $d\approx 6$ μm for the above parameters). In practice, coherence considerations (treated later) may preclude the use of the higher bands. However, for given u', higher spatial frequencies can be brought into contrast by decreasing z. An example is seen in Cloetens *et al.*[15] Ultimately detector resolution will impose an upper limit.

The effects of absorption if present will be added to the above (in our weak object approximation). For small u', cos $\chi\approx 1$, and (for pure absorption)

$$I(x)\approx 1-2m(x) \tag{18}$$

giving the usual shadow image, with maximum contrast at $z=0$ for all spatial frequencies (contact radiograph). As is clear from Eq. (8) or Fig. 1, absorption will in general complement phase contrast, i.e., for a given spatial frequency range one or another type of contrast will typically predominate.

Now we consider a point source of illumination instead of a plane wave. Let the object plane be a distance R_1 from the source, with the image plane situated at a further distance R_2. Equation (1) now becomes, apart from a constant,

$$f_s(x;R_1,R_2)=\left(\frac{i}{\lambda R_2}\right)^{1/2}\exp(-ikR_2)\int\exp\left(-ik\,\frac{X^2}{2R_1}\right)\times q(X)\exp\left(\frac{-ik(x-X)^2}{2R_2}\right)dX \tag{19}$$

in an obvious notation. It is readily shown[2] that, apart from constants and factors of unit modulus, the wave function f_s can be simply expressed in terms of that produced by plane wave illumination, f_p:

$$f_s(x;R_1,R_2)=f_p(x/M;R_2/M) \tag{20}$$

and in Fourier space

$$F_s(u;R_1,R_2)=F_p(Mu;R_2/M), \tag{21}$$

where $M=(R_1+R_2)/R_1$ is the magnification factor. For $R_2\ll R_1$ this reduces essentially to the plane-wave case (with $z=R_2$) but for $R_2\gg R_1$ we have

$$f_s(x;R_1,R_2)\approx f_p(R_1x/R_2;R_1). \tag{22}$$

That is, the ''focusing'' is determined by R_1, the magnification by R_2/R_1. This suggests that this configuration may be a suitable basis for an x-ray phase-contrast microscope. In principle one could, by decreasing R_1, bring high spatial frequencies into contrast (i.e., increase phase-contrast resolution) while simultaneously maintaining magnification to allow for detector resolution. For example, for $\lambda=0.1$ nm, $R_1=R_2=0.5$ m, maximum phase contrast occurs at $u=1.4\times 10^5$ m^{-1} (i.e., $d=7$ μm), where it should be noted that these values are referred to the object. This is slightly better than the resolution for the corresponding plane-wave case (i.e., for $z=0.5$ m) but, because of the $\times 2$ magnification, the detector resolution need only be ~ 14 μm. For 1 μm resolution R_1 should be 5 mm with, say, $R_2=50$ mm giving $\times 11$ magnification allowing a detector of 10 μm resolution. For 0.1 μm resolution, R_1 becomes 50 μm, so that a practical limit may be reached due to geometrical and mechanical constraints, quite apart from other factors to be now considered.

III. COHERENCE

So far a perfectly coherent source (plane or spherical wave) has been assumed. In practice a plane wave will have angular divergence α, representing a bundle of plane waves incident on the object. Now, for off-axis incidence Eq. (1) is modified in that $q(X)$ is multiplied by $\exp(-ikX\sin\theta)$, where θ is the angle of incidence. It follows that for small θ, $f(x)$ is shifted to $f(x-\theta z)$, and so also is $I(x)$, just as in geometrical optics. So for partially coherent illumination, each image point is convoluted with a point-spread function (PSF) of width αz, whose exact shape depends on the distribution of illumination intensity with angle. Equating this width with the inverse of the spatial frequency optimally transferred at this z, viz $(2\lambda z)^{1/2}$, gives

$$\alpha^2 z=2\lambda \tag{23}$$

as obtained by Cloetens *et al.*[15] This gives an estimate $\alpha/2\lambda$ for the lowest spatial frequency which can be observed with optimal contrast under these conditions: higher spatial frequencies can always be brought into (optimal) contrast by decreasing z. The inverse of this, viz $2\lambda/\alpha$, is the ''coherence width.''[1–3] (Different authors give different numerical coefficients, according to their coherence criteria). This coherence width is roughly the maximum distance between two object points for which interference effects will be observable. It is not necessary for the whole object or field of view to be coherently illuminated.

In terms of the OTF, convolution of Eq. (7) with the PSF is equivalent to multiplying Eq. (8) by its FT. This could, for example, be represented in Fig. 1 by an envelope which damps out the higher spatial frequencies, and gives an approximate high frequency limit above which information about the object cannot be obtained with these imaging conditions, the so-called ''information limit.'' But note that this

envelope varies relative to the OTF when plotted as a function of u for different z values. Specifically, as z decreases, the OTF goes to higher frequencies as $z^{-1/2}$, but the envelope asymptotes as z^{-1} (since it is the FT of a function of width proportional to z) so optimal contrast at higher frequencies can be reached by decreasing z, as previously noted.

For a partially coherent pointlike source (spherical wave), the ideal point source is spread over a finite area. If, in Eq. (16), $\exp(-ikX^2/2R_1)$ is replaced by $\exp[-ik(X-a)^2/2R_1]$, it is readily seen that the image is shifted laterally by R_2a/R_1. Thus if s is the source spread function, the image PSF will be R_2s/R_1, but when referred to the object this is reduced by M i.e., to $R_2s/(R_1+R_2)$. For $R_2 \ll R_1$ this again reverts to the plane-wave case, if α is identified with s/R_1, the angular width of the source at the object. For $R_2 \gg R_1$ the PSF tends to s; thus for the ''microscope'' configuration, resolution will be limited to the source size. This, with the associated problem of intensity, will undoubtedly be the greatest limitation of such a microscope. Optimal contrast for the corresponding spatial frequency $u=1/s$ occurs at

$$R_1 = s^2/2\lambda. \tag{24}$$

In this case lower spatial frequencies can be brought into (optimal) contrast by increasing R_1.

Next we consider the effect of chromatic coherence, the discussion of which will apply to both plane and spherical waves, by invoking Eqs. (20) or (21), as required. Suppose the source has a normalized intensity distribution, $w(\lambda)$. For a pure phase object one then has, from Eq. (7)

$$I(x) = 1 - \int [2\phi(x;\lambda) * (\mathcal{F} \sin \chi)(x;\lambda)] w(\lambda) d\lambda \tag{25}$$

and Eq. (9) then becomes

$$F(u) = \delta(u) - \int \Phi(u;\lambda) \sin(\pi\lambda z u^2) w(\lambda) d\lambda. \tag{26}$$

For example, if $w(\lambda)$ has the Gaussian distribution

$$w(\lambda) = \frac{1}{\sqrt{\pi}\Delta\lambda} \exp[-(\lambda-\lambda_0)^2/(\Delta\lambda)^2] \tag{27}$$

on using Eq. (13) we obtain

$$F(u) = \delta(u) - \frac{r_e}{\sqrt{\pi}\Delta\lambda} R(u) \int \lambda \sin(\pi\lambda z u^2) \times \exp[-(\lambda-\lambda_0)^2/\Delta\lambda^2] d\lambda, \tag{28}$$

where $R(u)$ is the FT of $\rho_e(x)$. The integral can be evaluated, giving

$$F(u) = \delta(u) - r_e R(u) \exp[-(\tfrac{1}{2}\pi z u^2 \Delta\lambda)^2] \times [\lambda_0 \sin(\pi\lambda_0 z u^2) + \tfrac{1}{2}\pi z u^2 (\Delta\lambda)^2 \cos(\pi\lambda_0 z u^2)]. \tag{29}$$

The second term on the right-hand side is simply $\Phi(u;\lambda_0) \sin\chi$, multiplied by an exponential damping function. This function decreases to ~ 0.5 for $u=(2\Delta\lambda z)^{-1/2}$. For u up to the ''passband'' value $u=(2\lambda_0 z)^{-1/2}$ it follows that one could have a wavelength spread $\Delta\lambda \sim \lambda_0$ without undue damping. This represents a large wavelength spread, and justifies (at least for this example) our earlier qualitative remarks regarding polychromatic sources. Note however the very rapid cutoff with increasing u, due to its fourth power in the exponent. Thus for a 50% increase in u above the value $(2\Delta\lambda z)^{-1/2}$, the exponential decreases from 0.54 to 0.04, and doubling u decreases it to 5×10^{-5}. Thus some monochromatization would seem to be required for high resolution; for instance in this latter case $\Delta\lambda \sim \lambda_0/4$ would restore the damping to the 0.5 level. Since λ cannot in fact be less than zero, some such restriction on $\Delta\lambda$ is physically reasonable even without explicit monochromatization. The last term on the right-hand side, arising from the λ dependence of Φ, can be included as a further modification of the OTF. For u not too great, this consists of replacing λ_0 in χ by $\lambda_0[1+1/2(\Delta\lambda/\lambda_0)^2]$.

The above results are essentially unchanged if absorption is included, although details of the correction terms differ due to the different λ dependence of μ. Calculations using a Lorentzian distribution

$$w(\lambda) = \frac{\Delta\lambda}{\pi} \frac{1}{(\lambda-\lambda_0)^2 + (\Delta\lambda)^2} \tag{30}$$

give an essentially similar result, viz. the main effect on the OTF is multiplication by a damping function, in this case $\exp(-\pi z u^2 \Delta\lambda)$.

IV. DISCUSSION AND ILLUSTRATIVE RESULTS

Many of the foregoing results may be summarized with the help of the following figures. Figures 2 and 3 show regions of visibility of spatial frequencies for a phase object as a function of $\log(z/\lambda)$ and $\log(u\lambda)$, where z equals R_2 for plane waves (Fig. 2) and R_1 for spherical waves (Fig. 3). This choice of variables gives one universal diagram for phase contrast, and one for amplitude contrast, on which specific coherence conditions can be added as described below. The particular numerical ranges given in the figures

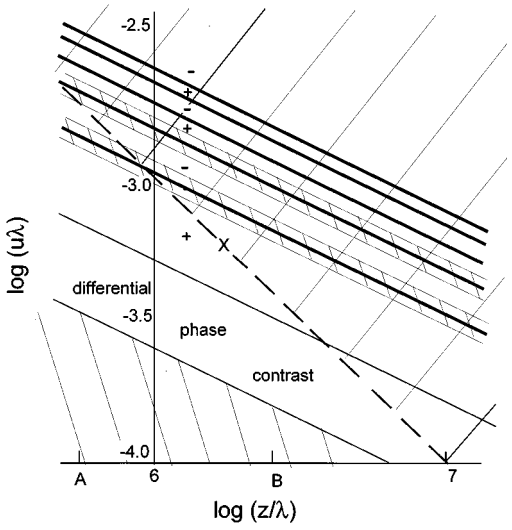

FIG. 2. Regions of visibility of a *phase-contrast image* in the z-u plane for effective *plane-wave conditions*. $z=R_2$ is the object-image distance.

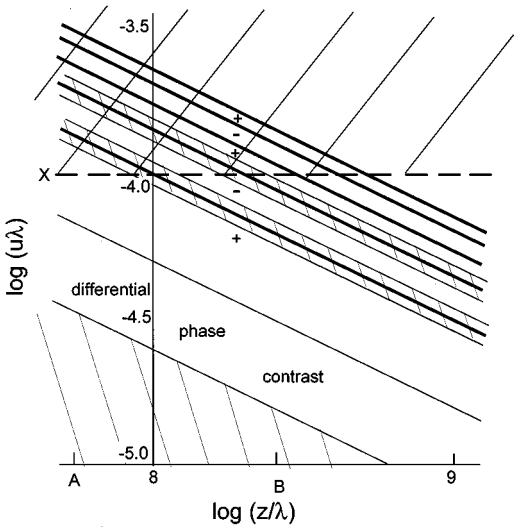

FIG. 3. Regions of visibility of a *phase-contrast image* in the z-u plane for effective *spherical-wave conditions*. $z=R_1$ is the source-object distance.

would be appropriate for typical coherence conditions for the hard x-ray region, $\lambda \sim 0.1$ nm. Visibility as the term is used in the present context allows for both contrast, as given by the OTF, and blurring, as determined by lateral coherence. Chromatic coherence is considered of lesser importance for reasons given above. Shaded regions indicate significantly reduced or absent visibility; it is to be understood however that the different regions are not sharply delineated, but merge into one another.

The zeroes of the OTF vary as $z^{-1/2}$. Due to finite detector sensitivity and noise, there will be a region of low visibility around each zero, and these are indicated by shaded areas for the first one or two zeroes and by heavy lines when they become closely spaced. In addition to these absent bands, u has both upper and lower limits, the latter due to the fact that the OTF starts at zero for $u=0$. The adjacent region of differential phase-contrast represents the region where the OTF varies as u^2. Note that this lower limit does not represent the largest visible features but rather spatial frequency content. Thus for example fibers and bubbles are visible by edge contrast,[16] but also more complex structures, e.g., fish[16] or bone[15] due to the spatial frequencies of their microstructure. The successive transfer bands are marked + and − for positive and negative contrast, according to the sign of the OTF.

The upper limit to u, representing the information limit

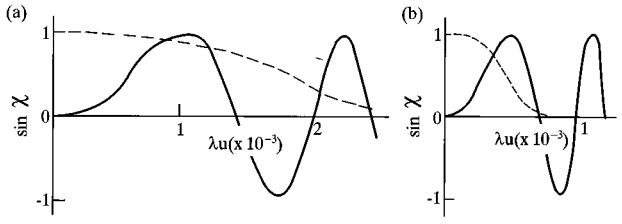

FIG. 4. (a)(b) Phase-contrast optical transfer function ($\sin \chi$) and coherence envelope (dashed line) vs spatial frequency λu for the *plane-wave case* for the two values of z/λ, A and B respectively, shown in Fig. 2.

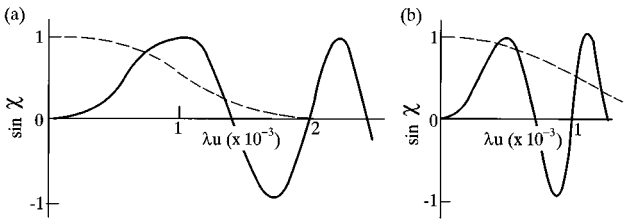

FIG. 5. Phase-contrast optical transfer function ($\sin \chi$) and coherence envelope (dashed line) vs spatial frequency λu for the *spherical-wave case* for the two values of z/λ, A and B respectively, shown in Fig. 3.

to resolution,[3] is given by the coherence envelope. On the figures this limit is shown by a dashed line. For the plane wave case it varies as $1/\alpha z$. Figure 2 shows the line for $\alpha = 10^{-3}$. The point X corresponds to the condition of Eq. (23). For the spherical wave case the limit is a constant, $1/s$, and is plotted as $\log(\lambda/s)$ in Fig. 3. The case shown would represent, say, $s=1\ \mu$m for $\lambda=0.1$ nm. The point X here indicates the condition of Eq. (24).

Two values of $\log(z/\lambda)$, namely A and B with $A<B$, are indicated in Figs. 2 and 3, and for each value the OTF and coherence envelope are shown as functions of λu, in Figs. 4(a) and 4(b) and 5(a) and 5(b), respectively. Note how lower frequencies are passed as z increases; and, in the plane-wave case, higher frequencies as R_2 decreases, since, as previously noted, the range of the coherence envelope increases faster than that of the OTF. In the spherical-wave case the source size sets a constant upper limit on spatial frequencies for all R_1, so that there will be a range of R_1, as given approximately by Eq. (24), such that the first band falls substantially within the coherence envelope; this will be the microscopy regime. For larger R_1 there will again be increased transfer at relatively low frequency, especially in the differential phase-contrast region; but also more OTF zeroes within the envelope [Fig. 5(b)]. This regime might be termed phase-contrast microradiography rather than microscopy.

For comparison, the corresponding data for an amplitude

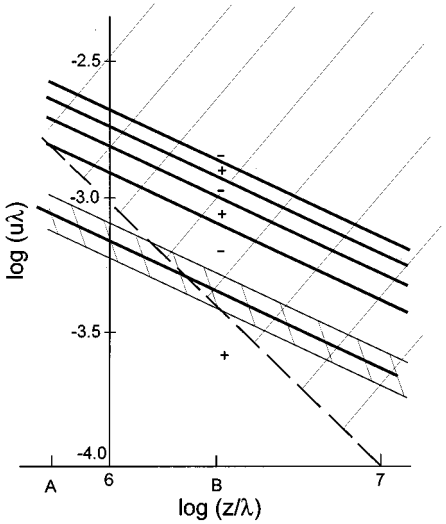

FIG. 6. Regions of visibility of an *amplitude contrast image* in the z-u plane for effective *plane-wave conditions*. $z=R_2$ is the object-image distance.

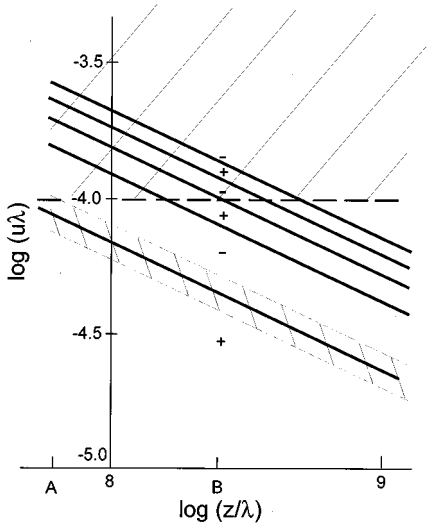

FIG. 7. Regions of visibility of an *amplitude contrast image* in the z-u plane for effective *spherical-wave conditions*. $z=R_1$ is the source-object distance.

object are given in Figs. 6–9. There is here no lower limit on u, as the OTF ($\cos\chi$) is unity at $u=0$, and optimum transfer for all frequencies occurs at $z=0$.

In general one may note that although various quantities associated with lateral coherence, such as the lateral coherence width and mutual coherence function,[1] are wavelength dependent, the effect on the resolution, as determined by the PSF or coherence envelope, depends only on geometrical factors, such as source size,[18] in the same way as for geometrical optics.

Finally there remains the question of retrieving object structure from the observed intensity of out-of-focus images. While largely outside the scope of this article, a few comments may be made here.

The problem can be logically divided into two parts. First, there is the recovery of the object transmission function, $q(x)$, including phase. This is relatively straightforward, and can be done holographically or otherwise (for example, via an appropriate form of the transport of intensity equations[39]). Then there is the generally more difficult problem of three dimensional object reconstruction. To obtain $q(x,y)$ for a three dimensional object, the projection approximation [Eq. (13) and its analogue for absorption] is useful and generally valid in the present context. A simple validity criterion[2] is that the object thickness should be less than about $d^2/2\lambda$, where d is the smallest resolvable dis-

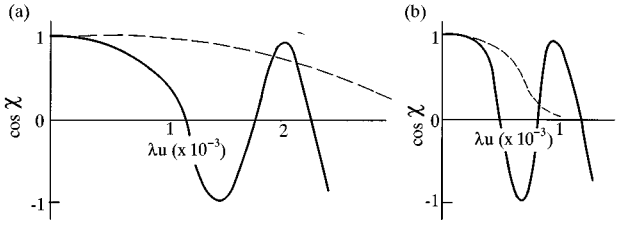

FIG. 8. (a)(b) Amplitude-contrast optical transfer function ($\cos\chi$) and coherence envelope (dashed line) vs λu for the *plane-wave case* for the two values of z/λ, A and B, respectively, shown in Fig. 6.

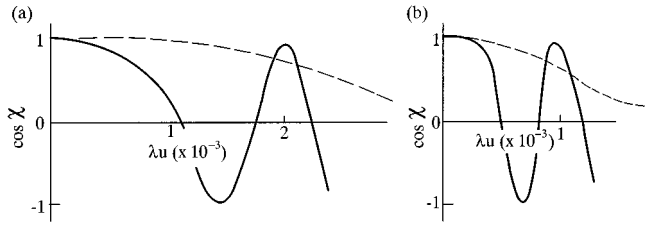

FIG. 9. (a)(b) Amplitude-contrast optical transfer function ($\cos\chi$) and coherence envelope (dashed line) vs λu for the *spherical-wave case* for the two of values of z/λ, A and B, respectively, shown in Fig. 7.

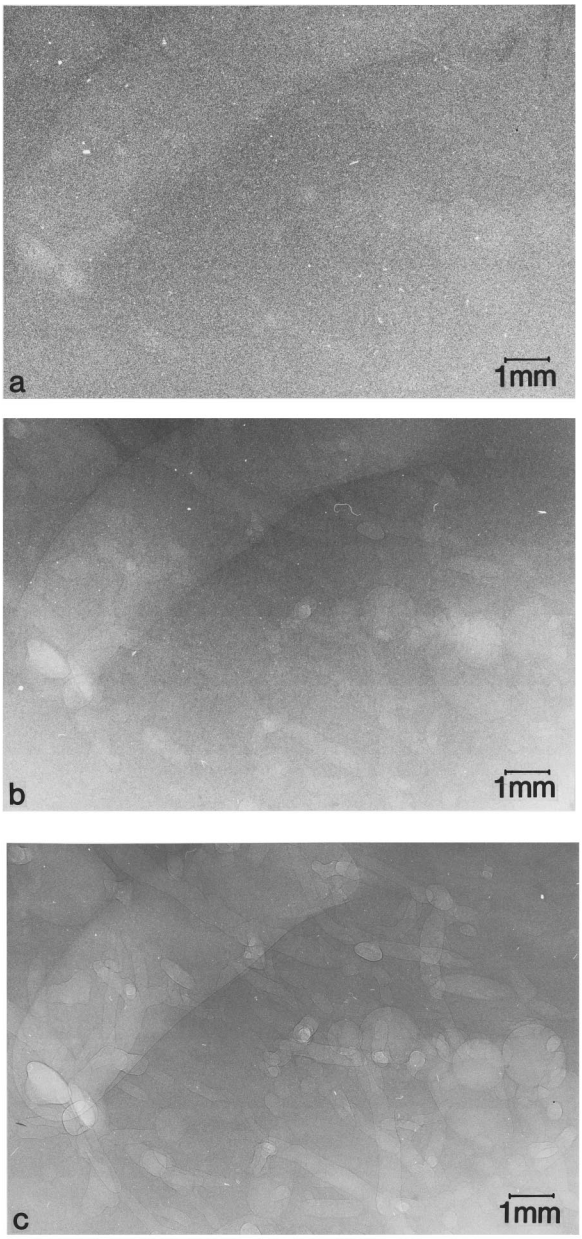

FIG. 10. Radiographs of a specimen of lamb's liver recorded with a microfocus source, showing phase contrast. R_1 was 300 mm and R_2 was; (a) 0 mm, (b) 300 mm, and (c) 1100 mm.

TABLE I. Summary of the characteristics of in-line imaging without lenses.

(A) General	
Advantages:	Simplicity of apparatus; i.e., no lenses or mirrors, no aberrations. Modest requirements for monochromaticity. Similar to present radiography systems. Reduced incoherent scattering contribution. Both amplitude and phase information can be derived from intensity data.
Disadvantages:	Source of high lateral coherence required. May require appropriate image-reconstruction procedure. Useful physical magnification limited by source size and closeness of approach of sample to source. No physical access to focal plane, which would allow employment of various contrast mechanisms. Increased sensitivity to the quality of in-beam components such as windows and filters.

Quantity of interest	Plane wave $R_1 \gg R_2$	Spherical wave $R_2 \gg R_1$
(B) Phase contrast		
Optimum contrast: $u=$	$(2\lambda R_2)^{-1/2}$	$(2\lambda R_1)^{-1/2}$
Coherence resolution limit: $u=$	$1/\alpha R_2$	$1/s$
Visibility, upper u limit:	None	$1/s$ with optimum contrast at $R_1=s^2/2\lambda$
Visibility, lower u limit: (This limit is considerably reduced when allowance is made for differential phase contrast.)	$\alpha/2\lambda$ (=coherence width^{-1}), with optimum contrast at $R_2=2\lambda/\alpha^2$	None (coherence width $=\lambda R_1/s$)
Limitations to high resolution:	Collimation, detector resolution, object-detector proximity	Source size, source-object proximity
(C) Absorption contrast		
Visibility, upper u limit:	None; provided $R_2 \ll 1/u\alpha$	$1/s$ arbitrary R_1
Visibility, lower u limit:	None	None
Limitations to high resolution:	Detector resolution, object-detector proximity.	Source size

tance. This means that Fresnel diffraction blurring in the object will not significantly degrade resolution. If projection is valid, tomographic methods can in principle be used for three dimensional reconstruction.

Much of the foregoing analysis has been based on the further assumption of the weak object approximation[2,3] [Eq. (4)] which has the advantages both of separating phase and amplitude contributions, and of linearizing the intensity expressions. The implied condition $\phi(x) \ll 1$ (and its absorption analogue) is, however, quite restrictive as a phase change of 2π is typically produced by a thickness difference of order a few tens of microns even for low Z materials, for x rays around 10 keV. In fact Guigay[43] has shown that, at least for a phase object, the inferred linearity properties such as Eqs. (6)–(8) hold under the condition

$$|\phi(x)-\phi(x-\lambda z u)| \ll 1, \tag{31}$$

which is much less restrictive, even though it is both z and u dependent. In any case, however, Eqs. (1) or (2) can always be used to calculate an image. The recovery of $q(x)$ from an image on the other hand will be more difficult if Eq. (4) [or more generally, Eq. (31)] is not applicable.

In terms of scattering theory, this represents a single-scattering approximation, although it does not exactly correspond to the usual kinematic theory of Fraunhofer diffraction in which the intensity is quadratic in ϕ, the difference being due to interference with the direct beam in the Fresnel case. This approximation improves with increasing energy, since ϕ decreases as λ [Eq. (13)]. For equivalent phase-contrast conditions, z must be increased to maintain constant λz. The projection approximation also improves, as is evident from its validity criterion relating to object thickness.

Plane- and spherical-wave illumination have been presented in this article as two limiting cases, but they are of course simply the extremes of all possible intermediate

cases. In particular, radiography is commonly performed with an (approximately) point source. So long as $R_2 \ll R_1$, the imaging will be of plane-wave type in terms of the foregoing theory. As R_2 is increased to values comparable to R_1, there will be an intermediate regime characterized by macroscopic, typically differential, phase contrast, modest magnification, and resolution somewhat smaller (i.e., better) than s, by a factor $R_2/(R_1+R_2)$ (apart from the effect of detector resolution). Such a regime may turn out to be useful in the design of clinical and industrial radiography systems, and has the further incidental, but possibly important advantage of reducing the contribution of scattered (typically Compton) radiation to the image, as practiced in the ''air-gap'' technique of radiography[44] sometimes used to reduce or eliminate the need for a grid (i.e., post-specimen collimation) while providing some magnification. It is perhaps also interesting to speculate that at least some of the improvement in contrast in some areas of conventional radiography, such as projection mammography with a very fine focus source, may have been due to phase-contrast effects rather than the simple reduction in scatter reaching the detector, as mentioned above.

Although the requirement of image reconstruction has been given here as a disadvantage of lenseless imaging compared with more direct methods, this does not mean that images cannot usefully be viewed directly. In fact, particularly in the macroscopic, differential phase-contrast imaging regime, readily interpretable object features may be visible and even enhanced.[16] In the context of electron microscopy, for instance, one distinguishes a directly interpretable ''point resolution limit,'' extending in spatial frequency to the first zero of the (phase-contrast) OTF, from the ''information limit'' determined by the coherence envelope. Thus in the x-ray case, at least in the area of qualitative radiography, the need for an image reconstruction step may prove to be more of an apparent than a real disadvantage.

Figure 10 provides an illustration of the foregoing comments. It shows radiographs of a specimen of lamb liver about 20 mm thick, taken with a microfocus source of nominal size 10 μm on a copper anode. The sample was not chemically fixed or treated in any way. R_1 was set at 300 mm, and R_2 was ~ 0, 300, and 1100 mm for Figs. 10(a), 10(b) and 10(c) respectively. Tube voltage was 60 kV, current 0.09 mA, and exposure times 2, 20, and 60 min., respectively using Agfa Curix film without an intensifying screen. After photographic enlargement, the final magnification for each panel of Fig. 10 is the same. Note the increase in contrast and resolution with increasing R_2, characteristic of differential phase contrast (the visible features are bile ducts). For normal absorption contrast radiography one would expect visibility to decrease with R_2 (unless resolution were strongly detector limited).

V. SUMMARY

The conditions and limitations for x-ray phase-contrast imaging by Fresnel diffraction have been considered. The methods can alternatively be considered as examples of in-line holography. The plane- and spherical-wave cases are treated as two extremes of a unified theory, appropriate for macroscopic imaging (radiography) and microscopy, respectively. Coherence requirements are considered and it has been shown that image resolution depends mainly on lateral coherence, with longitudinal (temporal or chromatic) coherence being of lesser importance. Resolution and contrast (together with signal/noise considerations which are not here treated in any detail) together determine the image *visibility* and information content. Corresponding results for absorption contrast are presented for comparison. Table I gives a summary of the main conclusions arising from the present work and may be best appreciated in conjunction with Figs. 2–9. For the type of microscopy considered in this article, source size is the basic limitation to resolution. Submicron microfocus tubes are becoming available, but their resolution has not yet approached the 10 nm range currently obtainable from soft x-ray direct imaging systems.[11,12] There is always the option of reducing magnification and using an ultrahigh resolution recording medium such as photoresist.[33] But the advantages of this type of microscopy are more likely to lie in its relative economy and simplicity compared to other methods which generally use either synchrotron or plasma sources together with elaborate optics. Even if resolution is not much better than for optical microscopy, the ability to study relatively thick, opaque specimens with minimal preparation requirements (particularly for biological samples) may provide sufficient motivation for its development. Phase-contrast (micro) tomography is a further possibility.[6,45] The general questions of image reconstruction and quantitative phase retrieval are left to future works.

ACKNOWLEDGMENT

The authors would like to thank Dr. Andrew Stevenson for helpful discussions.

[1] M. Born and E. Wolf, *Principles of Optics*, 6th ed. (Pergamon, Oxford, 1980).
[2] J. M. Cowley, *Diffraction Physics*, 3rd ed. (North Holland, Amsterdam 1995).
[3] J. C. H. Spence, *Experimental High-Resolution Electron Microscopy*, 2nd ed. (Oxford University Press, New York, 1988).
[4] U. Bonse and M. Hart, Appl. Phys. Lett. **6**, 155 (1965).
[5] M. Ando and S. Hosoya, in *Proceedings of the International Conference of X-Ray Optics and Microanalysis*, edited by G. Shinoda, K. Kohra and T. Ichinokawa (University of Tokyo Press, Tokyo 1972), p. 63.
[6] A. Momose, Nucl. Instrum. Methods Phys. Res. A **352**, 622 (1995).
[7] E. Forster, K. Goetz, and P. Zaumseil, Krist. Tech. **15**, 937 (1980).
[8] T. J. Davis, D. Gao, T. E. Gureyev, A. W. Stevenson, and S. W. Wilkins, Nature **373**, 595 (1995).
[9] D. Gao, T. J. Davis, and S. W. Wilkins, Aust. J. Phys. **48**, 103 (1995).
[10] V. N. Ingal and E. A. Beliaevskaya, J. Phys. D **28**, 2314 (1995).
[11] G. Schmahl, D. Rudolph, and P. Guttman in *X-Ray Microscopy II*, edited by D. Sayre, M. Howells, J. Kirz, and H. Rarback (Springer, Berlin, 1988), p. 228.
[12] G. Schmahl, D. Rudolph, G. Schneider, P. Guttman, and B. Niemann, Optik (Stuttgart) **97**, 181 (1994).
[13] Y. M. Hartman and A. A. Snigirev, in *X-Ray Microscopy IV*, edited by V. V. Aristov and A. I. Erko (Bogorodsky, Moscow, 1994), p. 429.
[14] A. Snigirev, I. Snigireva, V. Kohn, S. Kuznetsov, and I. Schelokov, Rev. Sci. Instrum. **66**, 5486 (1995).
[15] P. Cloetens, R. Barrett, J. Baruchel, J.-P. Guigay, and M. Schlenker, J. Phys. D **29**, 133 (1996).
[16] S. W. Wilkins, T. E. Gureyev, D. Gao, A. Pogany, and A. W. Stevenson, Nature (London) **384**, 335 (1996); S. W. Wilkins, Aust. Patent Application PN2112/95; PCT Patent Application PCT/AU96/00178 (1996).
[17] D. Gabor, Nature (London) **161**, 777 (1948).

[18] A. Baez, J. Opt. Soc. Am. **42**, 756 (1952).
[19] S. Kikuta, S. Aoki, S. Kosaki, and K. Kohra, Opt. Commun. **5**, 86 (1972).
[20] S. Aoki, Y. Ichihara, and S. Kikuta, Jpn. J. Appl. Phys. **11**, 1857 (1972).
[21] S. Aoki and S. Kikuta, Jpn. J. Appl. Phys. **13**, 1385 (1974).
[22] B. Reuter and H. Mahr, J. Phys. E **9**, 746 (1976).
[23] V. V. Aristov and G. A. Ivanova, J. Appl. Crystallogr. **12**, 19 (1974).
[24] V. V. Aristov, G. A. Bashkina, and A. I. Erko, Opt. Commun. **34**, 332 (1980).
[25] J. C. Solem and G. C. Baldwin, Science **218**, 229 (1982).
[26] M. R. Howells, in *X-ray Microscopy*, edited by G. Schmahl and D. Rudolph (Springer, Berlin, 1984), p. 318.
[27] M. R. Howells, M. A. Iarocci, and J. Kirz, J. Opt. Soc. Am. A **3**, 2171 (1986).
[28] M. R. Howells, C. Jacobsen, J. Kirz, R. Feder, K. McQuaid, and S. Rothman, Science **238**, 514 (1987).
[29] J. E. Trebes, S. B. Brown, E. M. Campbell, D. L. Mathews, D. G. Nilson, G. F. Stone, and D. A. Whelan, Science **238**, 517 (1987).
[30] D. Joyeux, S. Lowenthal, F. Polack, and A. Bernstein, in Ref. 11, p. 246.
[31] C. Jacobsen, J. Kirz, M. R. Howells, K. McQuaid, S. Rothman, R. Feder, and D. Sayre, in Ref. 11, p. 253.
[32] M. R. Howells, in Ref. 11, p. 263.
[33] C. Jacobsen, M. R. Howells, J. Kirz, and S. Rothman, J. Opt. Soc. Am. A **7**, 1847 (1990).
[34] I. McNulty, J. Kirz, C. Jacobsen, E. H. Anderson, M. R. Howells, and D. P. Kern, Science **256**, 1009 (1992).
[35] I. McNulty, Nucl. Instrum. Methods Phys. Res. A **347**, 170 (1994).
[36] G. Liu and P. D. Scott, J. Opt. Soc. Am. A **4**, 159 (1987).
[37] R. P. Millane, J. Opt. Soc. Am. A **7**, 394 (1990).
[38] M. Nieto-Vesperinas, *Scattering and Diffraction in Physical Optics* (Wiley, New York, 1991).
[39] T. E. Gureyev, A. Roberts, and K. A. Nugent, J. Opt. Soc. Am. A **12**, 1932 (1995).
[40] V. E. Coslett, A. Engstrom, and H. H. Pattee, *X-Ray Microscopy and Microradiography* (Academic, New York, 1957).
[41] V. E. Coslett and W. C. Nixon, *X Ray Microscopy* (Cambridge University Press, 1960).
[42] J. M. Cowley and A. F. Moodie, Proc. R. Soc. London **76**, 378 (1960).
[43] J-P. Guigay, Optik (Stuttgart) **49**, 121 (1977).
[44] S. C. Bushong, *Radiologic Science for Technologists*, 4th ed. (C. V. Mosby, St. Louis, Missouri, 1988).
[45] C. Raven, A. Snigirev, I. Snigireva, P. Spanne, A. Souvorov, and V. Kohn, Appl. Phys. Lett. **69**, 1826 (1996).